Grouping behavior of coaxial settling particles in a narrow channel

Deming Nie,[1] Jianzhong Lin,[1,2,*] and Rongqian Chen[1]
[1]*Institute of Fluid Mechanics, China Jiliang University, Hangzhou, 310018, China*
[2]*State Key Laboratory of Fluid Power Transmission and Control, Zhejiang University, Hangzhou 310027, China*
(Received 8 August 2015; published 12 January 2016)

Using numerical simulations, we studied the grouping behaviors of particles settling along their line of centers in narrow channels having a Reynolds number range of $5 \leqslant \mathrm{Re} \leqslant 50$. The calculations are based on our previously developed lattice Boltzmann direct-forcing–fictitious-domain method. We report the grouping behavior and investigate the dependence on the number of particles n, the initial interparticle separation h_0, and the Reynolds number Re. In particular, the mode of grouping is found to be independent of the number of particles when the Reynolds numbers is small. The two lowermost particles always come together first and form a vertical doublet and then the next two lowest particles form another doublet, and so on. Therefore, we observe $n/2$ doublets or $(n-1)/2$ doublets when n is even or odd, respectively. The uppermost particle is always left behind when n is odd. Furthermore, the separation between these doublets remains constant, displaying a power-law dependence decreasing from top to bottom.

DOI: 10.1103/PhysRevE.93.013114

I. INTRODUCTION

Particulate flows are found in numerous natural situations and industrial applications. Because of its academic and engineering importance, particle motion in fluids has been a long-lasting research topic. Understanding the interaction mechanisms among multiple particles is of considerable importance to gain insight into microstructural evolution in fluids, which is usually related to the collective behavior and self-organization of solid particles. The direct numerical simulation (DNS) method is a way of solving the problem of particle motion in fluids. In a DNS method, one must simultaneously integrate the Navier-Stokes equations (governing the motion of the fluid) and the equations of rigid-body motion (governing the motion of the particles). These equations are coupled through the no-slip condition on the particle boundaries, and through the hydrodynamic forces and torques that appear in the equations of rigid-body motion. In this paper, we simulate particle motion using a DNS method.

Fluid rheological behaviors and inertial effects may complicate the motion of particles in fluids. For instance, hydrodynamic interactions among particles mediated by the fluid are highly nonlinear even at a finite Reynolds number because of inertial effects, which are known to dramatically affect flow behavior [1–7]. Conversely, one of the unusual phenomena reported in viscoelastic suspensions is the formation of particle chains during sedimentation [8–12] and shear flows [13–16] as a result of normal stress differences. Riddle *et al.* [8] were the first to report this unexpected phenomenon, and observed that two spheres would chain with each other and form a stable two-particle cluster in some polymer solutions for small initial separations of the spheres. Recently, Hao *et al.* simulated the sedimentation of circular particles in a two-dimensional channel filled with an Oldroyd-B fluid using a fictitious-domain–distributed-Lagrange-multiplier method [12]. Even for a system with only six particles, they observed that particle chains are formed and move to the center of the channel when the elasticity number is greater than a critical value and the viscoelastic Mach number is less than 1 [12]. They also reported that the long chain falls faster than a single particle in the fluid.

However, in this work we report similar behavior for particles settling along their line of centers in a Newtonian fluid at a finite Reynolds numbers. We call this type of behavior "grouping" to distinguish it from "aggregation" in a non-Newtonian fluid. Similar problems have been extensively studied and the settling velocity can be analytically calculated in the case of a creeping flow [17]. However, the motion of particles is much more complex if we take into account the inertia effect. For instance, the well-known drafting-kissing-tumbling (DKT) motion could take place when multiple particles are settling at finite Reynolds numbers, resulting from hydrodynamic interactions. Conversely, if the particles are placed coaxially and released under only the influence of gravity at finite Reynolds numbers, it will take a very long time to observe DKT motion. Our work shows that, before the onset of DKT motion, the settling particles may display different grouping behaviors according to the Reynolds number as well as the initial conditions. In other words, the settling particles may be separated into several groups resulting from interparticle hydrodynamic interactions. Each group sediments at the same velocity overall. This behavior appears not to have been documented yet in a quantitative way. For instance, two kinds of behaviors are observed for three identical particles falling along their line of centers in a long channel. When the Reynolds number is small, the two lowermost particles form a doublet first and the uppermost particle is always left behind. Therefore, there are two groups of settling particles. However, the uppermost particle will catch up to the doublet to eventually form a triplet if the Reynolds number is large enough. In this case we can observe only one group. Undoubtedly, the presence of more particles can lead to more complex grouping behaviors. The interactions between particles can be complicated by inertial effects. Our results show that there are, in total, four kinds of grouping behaviors when four particles are settling in a channel. The influence of hydrodynamic interactions is considered to be crucial as

*Corresponding author: mecjzlin@public.zju.edu.cn

we have observed very unusual behaviors in the simulations, such as grouping of all the particles. A better understanding of this settling problem is nevertheless needed because it provides valuable insight into the hydrodynamic interactions among multiple particles at finite Reynolds number. In view of this, the primary purpose of this work is to show how the Reynolds number and the initial configurations affect the grouping behavior of the coaxial settling particles.

In this paper we simulate the settling of particles to study their grouping behavior, on account of interparticle hydrodynamic interactions, for the Reynolds number range $5 \leqslant \mathrm{Re} \leqslant 50$ and for the number of particles $n \leqslant 19$. The Reynolds number is defined as $\mathrm{Re} = \rho_f U_0 d/\mu$, where ρ_f and μ are the fluid density and dynamic viscosity, respectively, and d is the particle diameter. The reference velocity U_0 is chosen by equating the buoyancy-corrected weight of the object with a unit-coefficient drag force acting on the particle, which is given by $U_0 = [0.5\pi d(\rho_p/\rho_f - 1)g]^{-1}$ (in two dimensions) or $U_0 = [4d(\rho_p/\rho_f - 1)g/3]^{-1}$ (in three dimensions), where g is the gravitational constant and ρ_p is the density of a particle. For computational practicality, the results presented here are largely restricted to the case of two-dimensional (2D) particles, but we also present some three-dimensional (3D) results for spherical particles. The calculations are based on our previously developed lattice Boltzmann direct-forcing–fictitious-domain (LB—DF-FD) method [18]. In Sec. II, we present a brief outline of the LB—DF-FD method and define the problem. We then validate our method in Sec. III by comparing our results with previously reported data for several benchmark tests. In Sec. IV, we present our simulation results by first examining the grouping behaviors for $n = 4$. The effects of initial particle-particle separation and channel width are also considered. We then summarize the grouping behaviors for $n = 3 - 6$. Finally, we study the unique grouping behavior at low Reynolds numbers, which is independent of the number of particles. We present results and discussion for $n \leqslant 19$.

II. NUMERICAL METHOD

A. Lattice Boltzmann method

We solve the fluid flow problem using the lattice Boltzmann method (LBM). The discrete lattice Boltzmann equations of a single-relaxation-time model under external forces are expressed as [18]

$$f_i(\boldsymbol{x} + \boldsymbol{e}_i\Delta t, t + \Delta t) - f_i(\boldsymbol{x},t) = -\frac{1}{\tau}\left[f_i(\boldsymbol{x},t) - {f_i}^{(0)}(\boldsymbol{x},t)\right] + \frac{w_i\Delta t}{{c_s}^2}(\boldsymbol{\lambda}\cdot\boldsymbol{e}_i), \quad (1)$$

where $f_i(\boldsymbol{x}, t)$ is the distribution function for the microscopic velocity $\boldsymbol{e}_i$ in the ith direction, ${f_i}^{(0)}(\boldsymbol{x}, t)$ is the equilibrium distribution function, $\boldsymbol{\lambda}$ is the external force, Δt is the time step of the simulation, τ is the relaxation time, c_s is the speed of sound, and w_i are weights related to the lattice model. The fluid density ρ_f and velocity $\boldsymbol{u}$ are determined by the distribution function

$$\rho_f = \sum_i f_i, \quad \rho_f\boldsymbol{u} = \sum_i f_i\boldsymbol{e}_i. \quad (2)$$

For the two-dimensional, nine-velocity lattice model used here, the discrete velocity vectors are

$$\boldsymbol{e}_i = \begin{cases} (0,0), & \text{for } i = 0, \\ (\pm1,0)c, (0,\pm1)c, & \text{for } i = 1 \text{ to } 4, \\ (\pm1,\pm1)c, & \text{for } i = 5 \text{ to } 8, \end{cases} \quad (3)$$

where $c = \Delta x/\Delta t$ and Δx is the lattice spacing. The speed of sound $c_s^2 = c^2/3$. Following Qian [19], the equilibrium distribution function is

$${f_i}^{(0)}(\boldsymbol{x},t) = w_i\rho_f\left[1 + \frac{3\boldsymbol{e}_i\cdot\boldsymbol{u}}{c^2} + \frac{9(\boldsymbol{e}_i\cdot\boldsymbol{u})^2}{2c^4} - \frac{3\boldsymbol{u}^2}{2c^2}\right], \quad (4)$$

where w_i are set to $w_0 = 4/9$, $w_{1\text{–}4} = 1/9$, and $w_{5\text{–}8} = 1/36$.

By performing a Chapman-Enskog expansion, the macroscopic mass and momentum equations at the low-Mach-number limit can be recovered:

$$\frac{\partial\rho_f}{\partial t} + \nabla\cdot(\rho_f\boldsymbol{u}) = 0, \quad (5)$$

$$\frac{\partial(\rho_f\boldsymbol{u})}{\partial t} + \nabla\cdot(\rho_f\boldsymbol{u}\boldsymbol{u}) = -\nabla p + \mu\nabla^2\boldsymbol{u} + \boldsymbol{\lambda}, \quad (6)$$

where p is the pressure, $\boldsymbol{\lambda}$ is the pseudo–body force responsible for the motion of rigid bodies, and μ is the dynamic viscosity which can be expressed as $\mu = \rho_f(2\tau\text{–}1)(\Delta x)^2/6\Delta t$. For simplicity we set $\Delta x = 1$ and $\Delta t = 1$ in the present work.

B. Fluid-particle coupling

The fluid and solid particle are coupled by means of the fictitious-domain scheme [20]. In this method, the domains inside the particles are filled with the same fluid and satisfy the constraint of rigid-body motion. Therefore, the velocity is described by

$$\boldsymbol{u} = \boldsymbol{U} + \boldsymbol{\Omega}\times\boldsymbol{r} \text{ (the particle inner domain } P\text{)}, \quad (7)$$

where $\boldsymbol{U}$ and $\boldsymbol{\Omega}$ are the particle's translational and rotational velocities, respectively, and $\boldsymbol{r}$ is the position vector with respect to the particle's center of mass. Moreover, in this method, various Lagrangian nodes are needed to represent the particle, and a Eulerian mesh is used for the fluid.

The motion of a particle with mass M and moment of inertia $\boldsymbol{J}$ is governed by Newton's equations,

$$M\frac{d\boldsymbol{U}}{dt} = \boldsymbol{F}_H + \left(1 - \frac{1}{\rho_r}\right)M\boldsymbol{g} + \boldsymbol{F}_C, \quad (8)$$

$$\frac{d(\boldsymbol{J}\cdot\boldsymbol{\Omega})}{dt} = \boldsymbol{T}_H, \quad (9)$$

where ρ_r is the density ratio of particle to fluid. $\boldsymbol{F}_c$ is the collision force acting on the particle by other particles within a certain interparticle cutoff distance, which will be further discussed. $\boldsymbol{F}_H$ and $\boldsymbol{T}_H$ are the hydrodynamic forces and torques on the particle, respectively:

$$\boldsymbol{F}_H = \int_{\partial P}\boldsymbol{n}\cdot\sigma\, ds, \quad (10)$$

$$\boldsymbol{T}_H = \int_{\partial P}\boldsymbol{r}\times(\boldsymbol{n}\cdot\sigma)ds, \quad (11)$$

where σ is the fluid stress tensor and $\boldsymbol{n}$ is the unit outward normal on the particle surface. $\boldsymbol{F}_C$, the particle-particle

collision force, is described below. Based on a direct-forcing scheme, the force exerted on the Lagrangian points in the particle domain can be expressed as

$$\boldsymbol{\lambda}^{n+1} = \rho_f \frac{\boldsymbol{u}^{n+1} - \boldsymbol{u}^*}{\Delta t} = \rho_f \frac{\boldsymbol{U}^{n+1} + \boldsymbol{\Omega}^{n+1} \times \boldsymbol{r} - \boldsymbol{u}^*}{\Delta t}, \quad (12)$$

where $\boldsymbol{u}^*$ is a temporary velocity, which satisfies the momentum equation [Eq. (6)] with zero body force, and $\boldsymbol{\lambda}^{n+1}$ is the discrete form of the pseudo–body force in Eq. (6). In the interest of brevity, the specific numerical algorithms of the LB—DF-FD method are not explained here; they are described in detail in [18].

C. Particle-particle interactions

When two particles come into close contact with each other, the lubrication force becomes important. This force is caused by the attenuation of the fluid film in the gap between the two particles and is repulsive upon approach and attractive upon separation of the particles. However, when the gap between two particles is of the order of one lattice spacing, the lubrication force is not completely resolved with the lattice Boltzmann method. To solve this problem, we applied a lubrication force model proposed by Kromkamp *et al.* [21]:

$$\boldsymbol{F}_C = \begin{cases} 0, & h > \delta_c, \\ -\frac{1}{2}\mu \boldsymbol{U}_{12} \cdot \boldsymbol{R}_{12}{}' \left[\left(\frac{a_1+a_2}{h} \right)^{3/2} \left(F_0 + \frac{h}{a_1+a_2} F_1 \right) - \left(\frac{a_1+a_2}{\delta_c} \right)^{3/2} \left(F_0 + \frac{\delta_c}{a_1+a_2} F_1 \right) \right], & h < \delta_c, \end{cases} \quad (13)$$

Here a_1 and a_2 are the radii of the two particles. $\boldsymbol{U}_{12} = \boldsymbol{U}_1 - \boldsymbol{U}_2$, $h = |\boldsymbol{R}_{12}| - (a_1 + a_2)$ is the distance between the particle surfaces, and δ_c represents the cutoff distance between the particle surfaces for the added lubrication force, which is fixed at $\delta_c = 1.6\Delta x$ in the simulations. The unit vector $\boldsymbol{R}_{12}{}' = \boldsymbol{R}_{12}/|\boldsymbol{R}_{12}|$. According to Kromkamp *et al.* [21], F_0 and F_1 are two constants given by $F_0 = 3.3322$ and $F_1 = 12.829$. For a three-dimensional system, the lubrication force proposed by Nguyen and Ladd is adopted [22].

D. Problem definition

We consider the interactions of multiple settling particles that are initially located along the channel axis and then released under gravity. For simplicity, we consider only the case where all the particles are equally spaced. h_0 is defined as the initial interparticle separation which is the closest distance between two neighboring particles. The computational domain is $L \times H = 4d \times 400d$ (in two dimensions) or $L \times L \times H = 4d \times 4d \times 250d$ (in three dimensions). We believe that the height of the domain is large enough to allow the settling particles to reach a steady state. We choose no-slip boundary conditions on all four fixed walls of the domain. This avoids specifying the far-field boundary conditions on a finite computational domain. For the following, the parameters are fixed at $\rho_f = 1$, $\rho_p = 2$, and $d = 20$ (in lattice units).

III. VALIDATION

To demonstrate the use of the LB—DF-FD method and further validate its results, we compare our results with a previous immersed-boudary–LBM simulation of the well-known DKT motion [23]. In the simulations, the domain is 2 cm (x direction) × 8 cm (y direction), which corresponds to a computational domain of 200 × 800 lattice units. The fluid density is 1 g/cm^3, and the viscosity is 0.01g/cm s. The particle density is 1.01 g/cm^3, and the radius of the particles is 0.1 cm. Initially, the first particle is 0.001 cm off center of the channel axis at a height of 7.2 cm and the second particle is at the channel center at a height of 6.8 cm. The particles start settling in the y direction under the influence of gravity. For particle-particle interactions, we choose a collision technique proposed by Glowinski *et al.* [24]:

$$\boldsymbol{F}_C^{i,j} = \begin{cases} 0, & |\boldsymbol{X}_i - \boldsymbol{X}_j| > a_i + a_j + \zeta, \\ \frac{c_{ij}}{\varepsilon_p} \left(\frac{|\boldsymbol{X}_i - \boldsymbol{X}_j| - a_i - a_j - \zeta}{\zeta} \right)^2 \left(\frac{\boldsymbol{X}_i - \boldsymbol{X}_j}{|\boldsymbol{X}_i - \boldsymbol{X}_j|} \right), & |\boldsymbol{X}_i - \boldsymbol{X}_j| < a_i + a_j + \zeta. \end{cases} \quad (14)$$

According to Feng and Michaelides [23], the parameter c_{ij} is the force scale chosen to be the buoyancy force on the particle; ε_p is the stiffness parameter for collisions, which is usually taken to be $\varepsilon_p = \Delta x^2$; a_i and a_j are the radii of the i and j particles, respectively; and ζ is the range of the repulsion force which is taken to be $\zeta = 1.5\,\Delta x$. We summarize our comparisons in Fig. 1. It is shown that the present results are in good agreement with the immersed–boundary–lattice-Boltzmann method results [23]. We also present the results for $\varepsilon_p = \Delta x$ which are almost identical to those for $\varepsilon_p = \Delta x^2$.

To further validate our simulation method, a spherical particle settling in a square tube is simulated and compared with previous results. A spherical particle of diameter d is released in a vertical square channel of width L and settles under gravity. In the simulations, $d = 13$ and $\tau = 0.8$, and the Reynolds number is fixed at $\mathrm{Re}_\infty = 0.36$, which is based on U_∞, the unconfined terminal velocity from the Stokes equation. The sphere is initially released at the center of the cross section of the channel with zero velocity. The particle settles along the axis of the channel and reaches its terminal velocity. Due to the wall effects the terminal velocity will be less than the terminal velocity of an unconfined particle. As shown in Fig. 2(a), there is good agreement between previous results [25,26] and the present ones. The second case is the dependence of the Reynolds number Re_T, which is based on the terminal settling velocity U_T, on the ''best number"

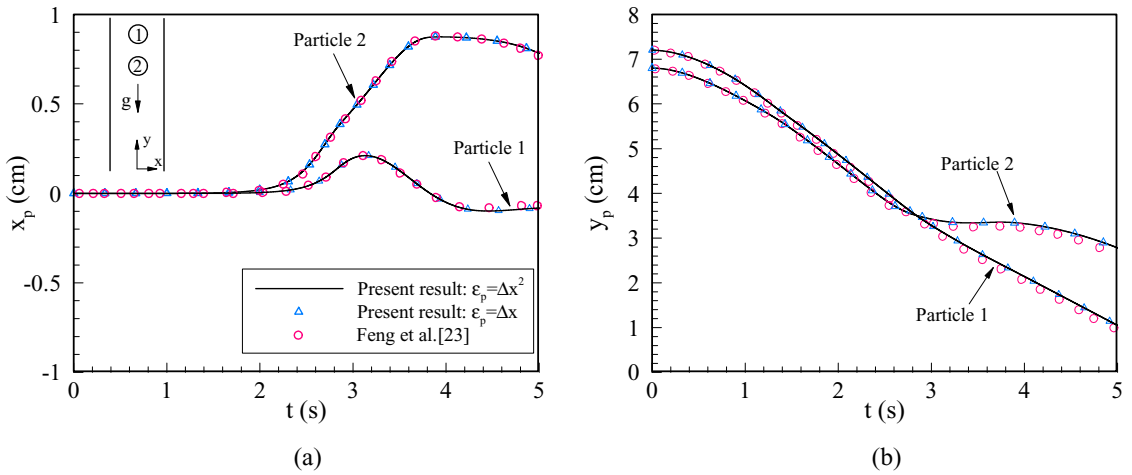

(a) (b)

FIG. 1. Comparison between previous results and the current simulations for drafting-kissing-tumbling (DKT) motion: (a) Transverse coordinates and (b) longitudinal coordinates of the two particles.

N_D [27]. N_D is given by $N_D = \mathrm{Re}^2$ and Re is the Reynolds number based on U_0. In this case, $d = 16$ and $\rho_r = 2$, and the computational domain is $80 \times 80 \times 960$. One can see a good agreement between previous results [20,27,28] and the present ones for $\mathrm{Re}_T < 100$ in Fig. 2(b).

IV. RESULTS

A. Grouping behaviors for $n = 4$

We detail the grouping behaviors (GBs) for $n = 4$ in this section. The initial interparticle separation and channel width are fixed at $h_0' = h_0/d = 1.5$ and $L' = L/d = 4$, respectively. In total, four distinct behaviors can be observed during particle settling by varying the Reynolds number. Typical streamline patterns, along with pressure distributions, are displayed in Fig. 3. For referencing convenience, we number the particles from top to bottom. The behaviors illustrated in Figs. 3(a) and 3(b), which show the results for $\mathrm{Re} = 15$ and $\mathrm{Re} = 25$, respectively, are qualitatively similar. In both cases particle 3 first comes closer to particle 4 and then particle 1 comes closer to particle 2, forming two separate vertical doublets. In the first case, however, the distance between these two doublets remains finite, while in the second case these two doublets eventually contact and form a four-particle cluster, which settles as a single cohesive unit. This can be further confirmed by examining the time history of normalized separations between the neighboring particles as seen in Figs. 4(a) and 4(b), which correspond to conditions in Figs. 3(a) and 3(b), respectively. We believe that the upper doublet is dragged into the wake of the lower doublet during settling, resulting from stronger hydrodynamic interactions for larger Reynolds numbers. For reference convenience in the following sections, we denote these two behaviors as "GB I" and "GB II," respectively.

At intermediate Reynolds numbers we observe a transient behavior, as shown in Fig. 3(c). The nature of the third case is utterly different because particle 2 first settles individually, rather than grouping with particle 1. The distance between

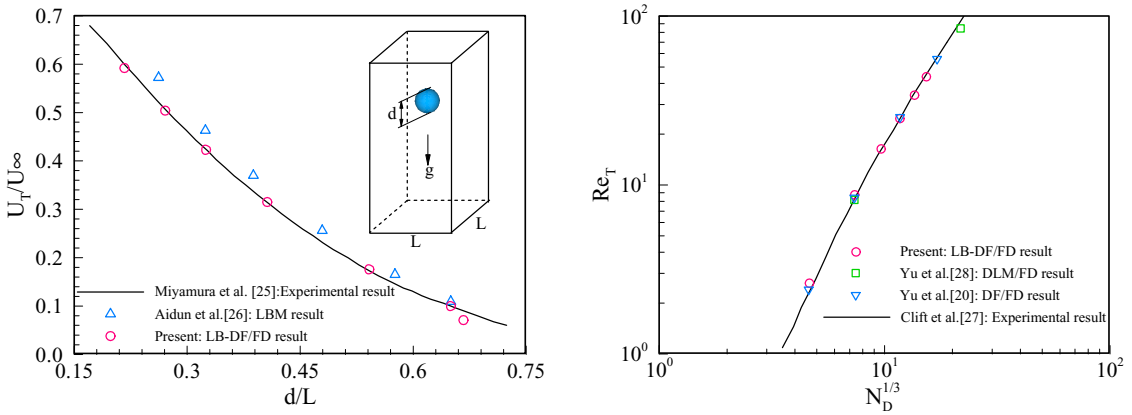

(a) (b)

FIG. 2. Comparison between previous results and the current simulations for a settling sphere along the axis of a square channel: (a) The dependence of the terminal settling velocity on the particle-wall distance ratio, (b) Re_T vs $N_D^{1/3}$. Re_T is the Reynolds number based on the terminal settling velocity, and N_D is called the "best number," which is given by $N_D = \mathrm{Re}^2$. U_∞ is the unconfined terminal velocity from the Stokes equation.

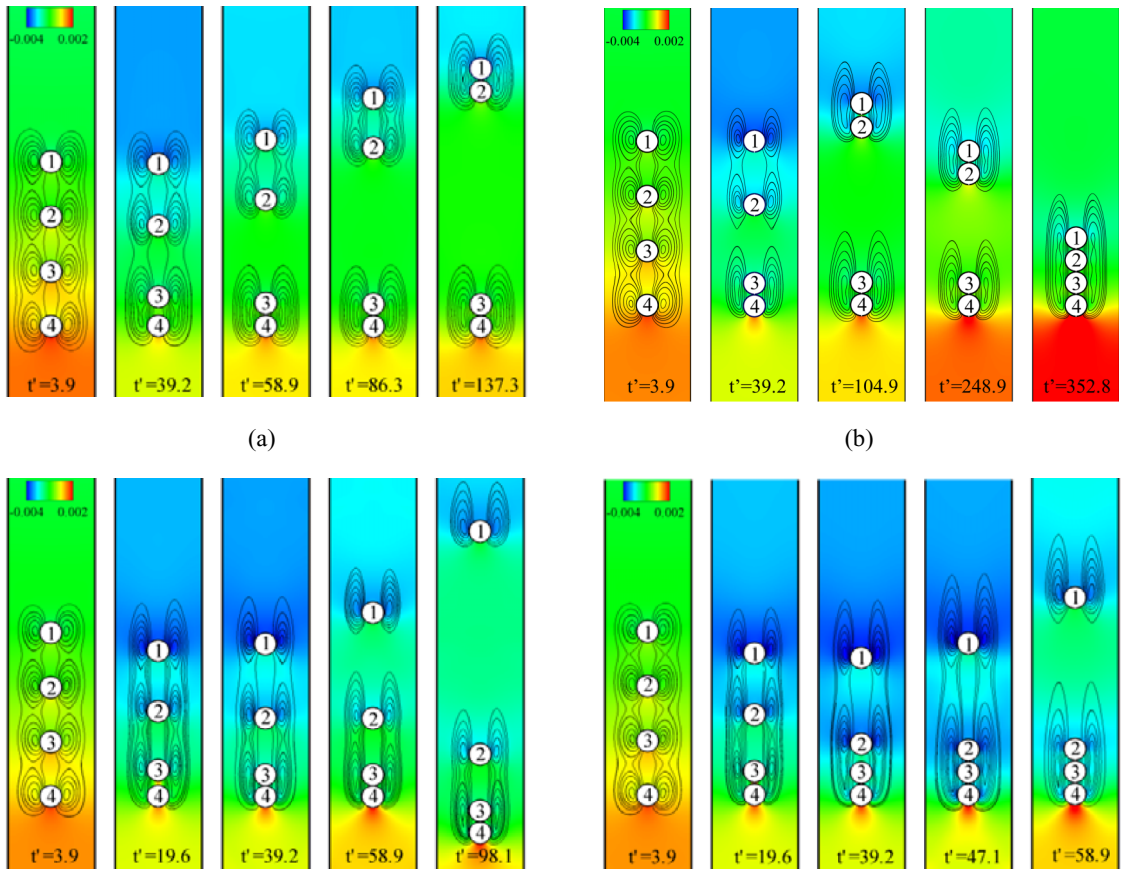

FIG. 3. Evolution of the settling behavior as the Reynolds number is increased: (a) Re = 15, (b) Re = 25, (c) Re = 32.7, and (d) Re = 40. The particles are consecutively numbered from the top to the bottom.

particle 1 and particle 2 remains constant, as shown in Fig. 4(c), while the distance between particle 2 and the doublet (particle 3 and particle 4) increases, because of the larger settling velocity of the latter. Furthermore, this behavior is rarely encountered in the simulations because we can observe it only when the Reynolds number is approximately 32.7 under the above-mentioned conditions. We call this type of behavior "GB III."

If the Reynolds number is large a different class of behavior is found: particle 3 and particle 4 form a doublet first and then particle 2 joins it quickly, which makes a triplet, resulting in an increase in the settling velocity. This leads to the fact that the trailing particle (particle 1) is always left behind, as shown in Fig. 3(d). We call this type of behavior "GB IV." While there are a total of four grouping behaviors that can manifest when varying the Reynolds number, the evolution of grouping behavior is not simply I $\rightarrow$ II $\rightarrow$ III $\rightarrow$ IV, as is discussed below.

In Fig. 4, we also present the results of the lubrication force model proposed by Yuan and Ball [29] with a cutoff distance of $\delta_c = 1.6\,\Delta x$. There are negligible differences between the results of these two models. Furthermore, to check the effect of the cutoff distance, we conduct corresponding simulations of $\delta_c = 2.0\,\Delta x$ for the lubrication force proposed by Kromkamp *et al.* [21]. As shown in Fig. 4, the effect of the cutoff distance δ_c is also negligible if $\delta_c \cong \Delta x$. We also examine the same problem using the repulsive force model [24]. From a qualitative point of view, all the results are comparable, despite the different mechanisms; therefore, we believe that the collision methods do not alter the essential features of the settling behavior of particles.

Figure 5 shows the normalized particle settling velocity over time for the different grouping behaviors seen in Fig. 3. For comparison, we also show the settling velocity of an isolated particle under the same flow conditions. It can be observed that the grouping behavior results in an increase in the settling velocity, which is consistent with previous experiments of three spheres settling in shear-thinning fluids [10,11]. This leads to the fact that the cluster may leave neighboring particles behind, as shown in Fig. 3(c). However, in some cases the reverse happens. The cluster may drag the neighboring particle into its wake and then form a larger cluster, as shown in Fig. 3(d).

Typically, the velocity of a doublet is more than 30% greater than that of an isolated particle, as shown in Figs. 5(a) and 5(c), while the velocity of a triplet is more than 60% greater than that of an isolated particle, as shown in Fig. 5(d).

For the behavior of GB I which is observed at low Reynolds number, two stable doublets always settle at the same velocity,

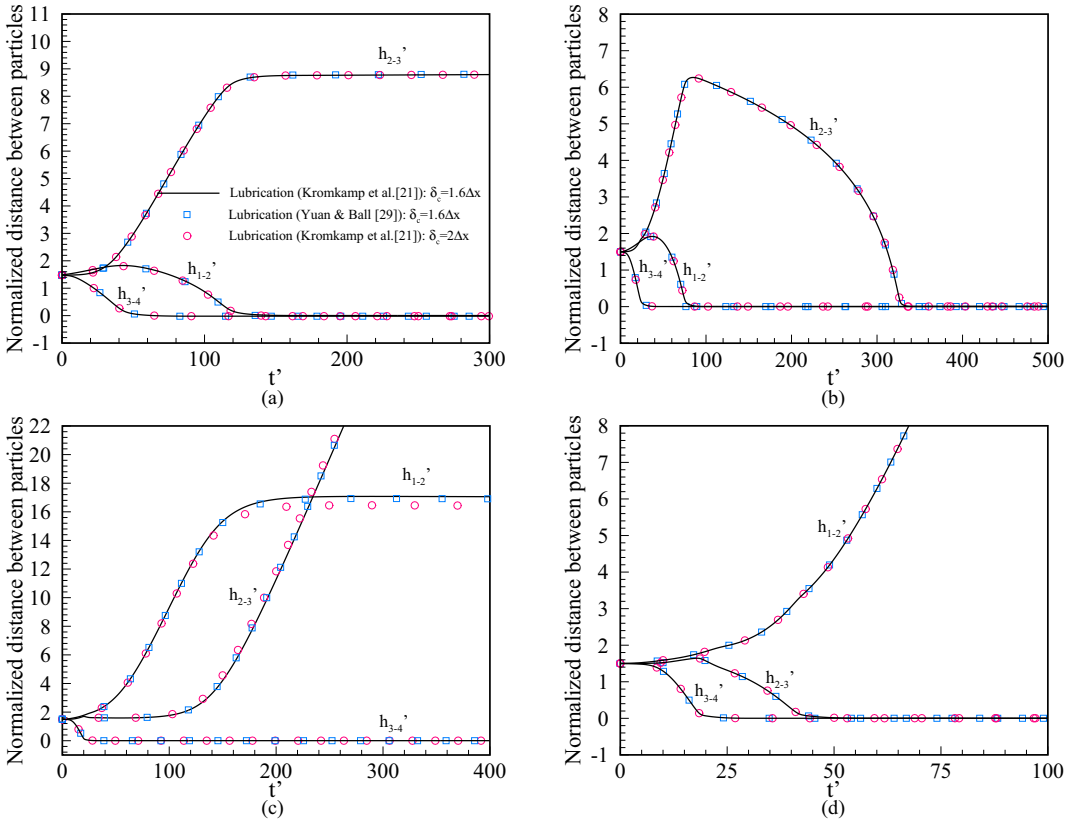

FIG. 4. Time history of normalized separations between neighboring particles for different grouping behaviors: (a) Re = 15 (GB I), (b) Re = 25 (GB II), (c) Re = 32.7 (GB III), and (d) Re = 40 (GB IV). $h'_{i\text{-}j}$ represents the separation between the surfaces of particles i and j which is normalized by the particle diameter d.

as shown in Fig. 5(a), which leads to a constant distance between the two doublets. To gain more insight into this kind of behavior, we also studied the effects of initial interparticle separation h'_0 and channel width L'. In Fig. 6, we show the final separation between particle 2 and particle 3 (i.e., the final distances between doublets) under different conditions. The distance between doublets decreases with increasing Reynolds number. The smaller the initial interparticle separation, the smaller the final distance between doublets. Furthermore, the effect of the walls is also remarkable, as shown in Fig. 6. The distance is larger when the walls are closer to the particles. This is because the walls suppress particle settling, which takes more time to form the doublets. To further investigate the effect of δ_c, we also present the results for $\delta_c = \Delta x$ and $\delta_c = 2.0\,\Delta x$ for $L' = 4$ and $h'_0 = 1.5$. As one can see in Fig. 6, there is little difference among the results when varying the value of δ_c. The same problem has also been solved by using the lattice Boltzmann method proposed by Lallemand and Luo [30], which treats moving boundaries in a different way. The results are also presented in Fig. 6, which shows agreement with the results by the present LB—DF-FD method [18].

We have done a detailed study of the effects of initial interparticle separation $h_0{}'$ as well as channel width L' on the grouping behavior, and summarize the results in Fig. 7. As previously mentioned, there are four different grouping behaviors, but the evolution of the grouping behavior is complex. For large value of $h_0{}'$, such as $h_0{}' > 1$, the settling of particles goes through five overall stages as the Reynolds number increases, i.e., I → II → I → III → IV, while it goes through four stages (I → III → IV → II) for small initial separations such as $h_0{}' < 1$. Furthermore, we observe six total stages (I → II → I → III → IV → II) for particle settling when $h_0{}' = 1$. As mentioned above, the GB III behavior is rarely observed because it takes place only at a specific Reynolds number which shows a linear relationship with the value of $h_0{}'$, as shown in Fig. 7(a). We believe that it can be regarded as a transient motion from I to IV. The effect of the walls on the settling behavior is also found to be significant, as shown in Fig. 7(b). The initial separation is fixed at $h_0{}' = 1.5$. We observe only two behaviors (I → II) when the particles are very close to the walls, i.e., $L' < 3.5$. Furthermore, the behavior of GB I is more likely to happen for small Reynolds number. However, particle settling becomes much more complex if the walls are distant from the particles, and five stages (I → II → I → III → IV) are seen as the Reynolds number increases.

To supplement and compare our two-dimensional results, we present some three-dimentional results for $h_0{}' = 1.5$ and $n = 4$ in Fig. 8. Similarly to the two-dimensional results shown in Fig. 3, we also observed four different behaviors when varying the Reynolds number. There is no qualitative difference between the 2D and 3D results except that for the behavior of GB I we observe much larger distances between doublets in three dimensions at similar Reynolds numbers. However, as the variations between the 2D and 3D results are

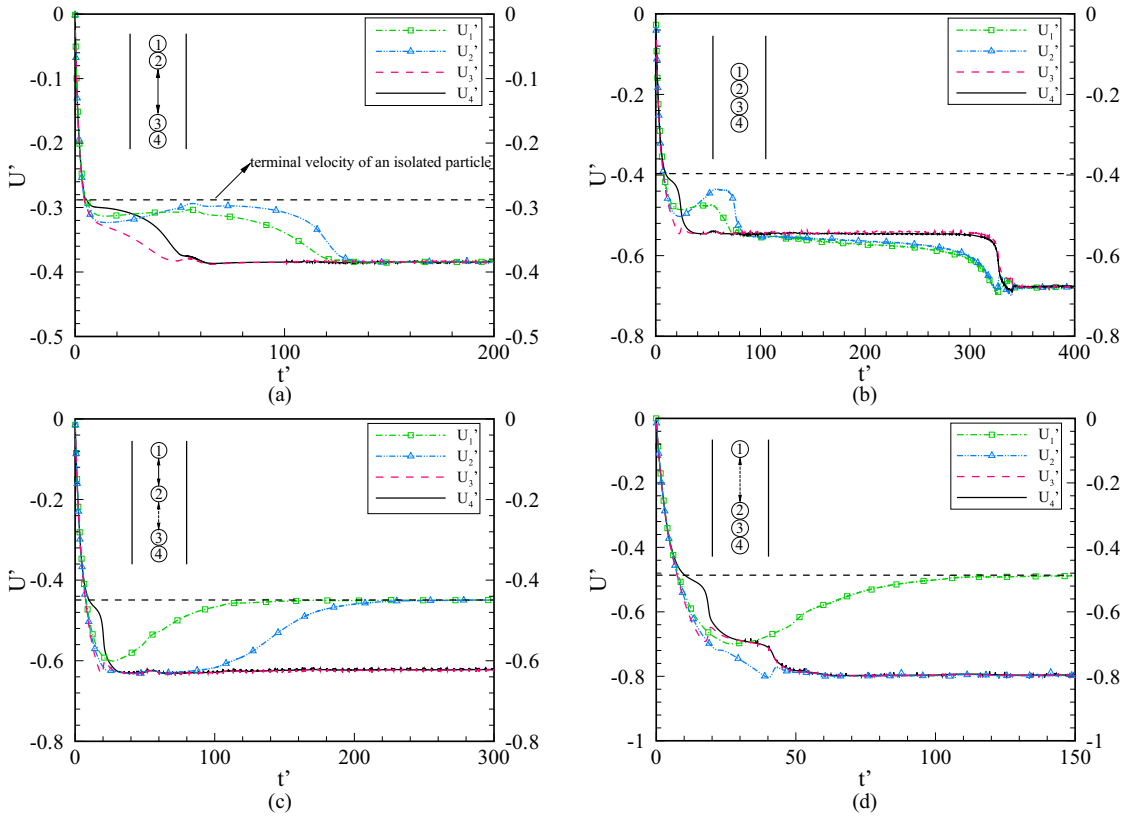

FIG. 5. Time history of normalized settling velocity for different grouping behaviors: (a) Re = 15 (GB I), (b) Re = 25 (GB II), (c) Re = 32.7 (GB III), and (d) Re = 40 (GB IV). The settling velocity is normalized by U_0.

not large, we do not intend to conduct more 3D simulations in the interest of computational practicality.

B. Summary of grouping behavior for $n = 3, 4, 5$, and 6

In addition to $n = 4$, we also studied the settling behavior of particles for $n = 3, 5$, and 6. The computational domain is $4d \times 500d$ for $n = 5$ and 6. We summarize all the results in Fig. 9. The initial separation is fixed at $h_0' = 1.5$. For the case of $n = 3$, shown in Fig. 9(a), particles 2 and 3 first cluster and leave behind particle 1 when the Reynolds number is small ($\mathrm{Re} \leqslant 37$), while particle 1 may catch up to the cluster to later form a vertical triplet at higher Reynolds numbers ($\mathrm{Re} \geqslant 38$). These two behaviors were also seen by Daugan *et al.* [10,11], who experimentally studied the settling of three spheres in a shear-thinning fluid at small Reynolds numbers.

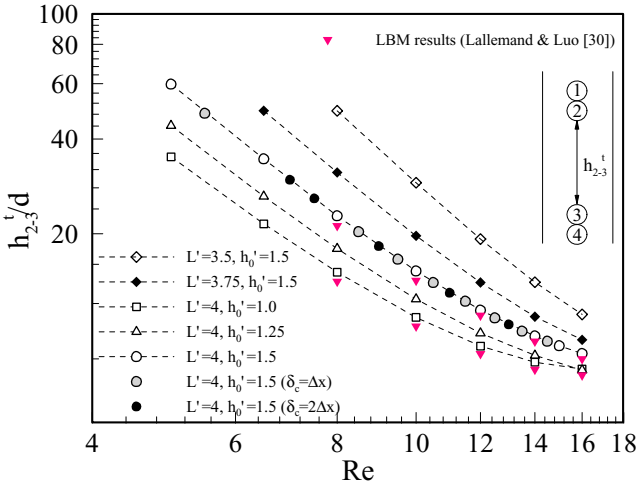

FIG. 6. Separation between particle 2 and particle 3 (i.e., the distances between doublets) at steady state under different conditions for GB I.

Figure 9(b) illustrates the evolution of settling behavior for $n = 4$, which is already shown in Fig. 7. Obviously, we can observe the behavior of GB I not only at low Reynolds numbers, i.e., $5 \leqslant \mathrm{Re} \leqslant 17$, but also at intermediate Reynolds numbers $32 \leqslant \mathrm{Re} \leqslant 32.6$. The most significant difference between these two regions is that the distance between doublets decreases with Re for the former, as shown in Fig. 6, while it increases for the latter. For instance, the distance is approximately $34d$ at $\mathrm{Re} = 32$ while it is more than $70d$ at $\mathrm{Re} = 32.6$. As mentioned above, particle 3 always comes close to particle 4 first and then particle 1 comes close to particle 2, forming two doublets. If the Reynolds number is large, such as $\mathrm{Re} \geqslant 32$, the lower doublet will sediment very fast due to strong inertial effects, leaving the upper one behind. However, the outcomes will be very different if the Reynolds number slightly increases. As seen in Fig. 9(b), particle 1 does not come into contact with particle 2 when $\mathrm{Re} \geqslant 32.72$, resulting from the hydrodynamic interactions with the lower doublet.

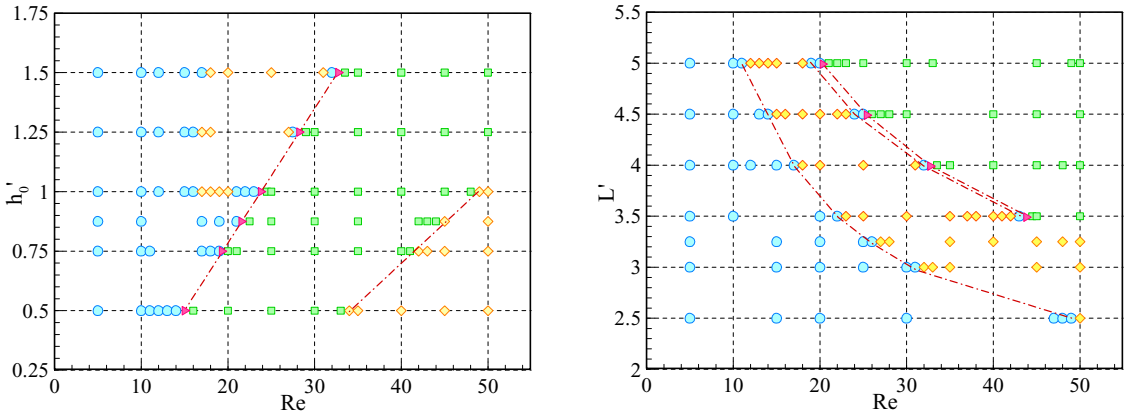

FIG. 7. Settling phase diagram for $n = 4$ as a function of (a) initial particle-particle separation and Reynolds number, and (b) channel width and Reynolds number. The symbols denote different behaviors: GB I (circles), GB II (diamonds), GB III (triangles), and GB IV (squares).

For the case of $n = 5$ shown in Fig. 9(c), five distinct grouping behaviors are observed. However, the particle settling goes through seven total stages as the Reynolds number increases, i.e., I → II → I → III → IV → V → II. Generally, the evolution of the settling behavior is similar to that of $n = 4$, except for behavior III shown in Fig. 9(c). In this case, the two lowermost particles (particles 4 and 5) first form a doublet, and particles 1 and 2 subsequently form another doublet. The upper doublet (particles 1 and 2) will catch up to particle 3 because of larger settling velocity, leading to a triplet. For the same reason, the triplet catches up to the lower doublet, and

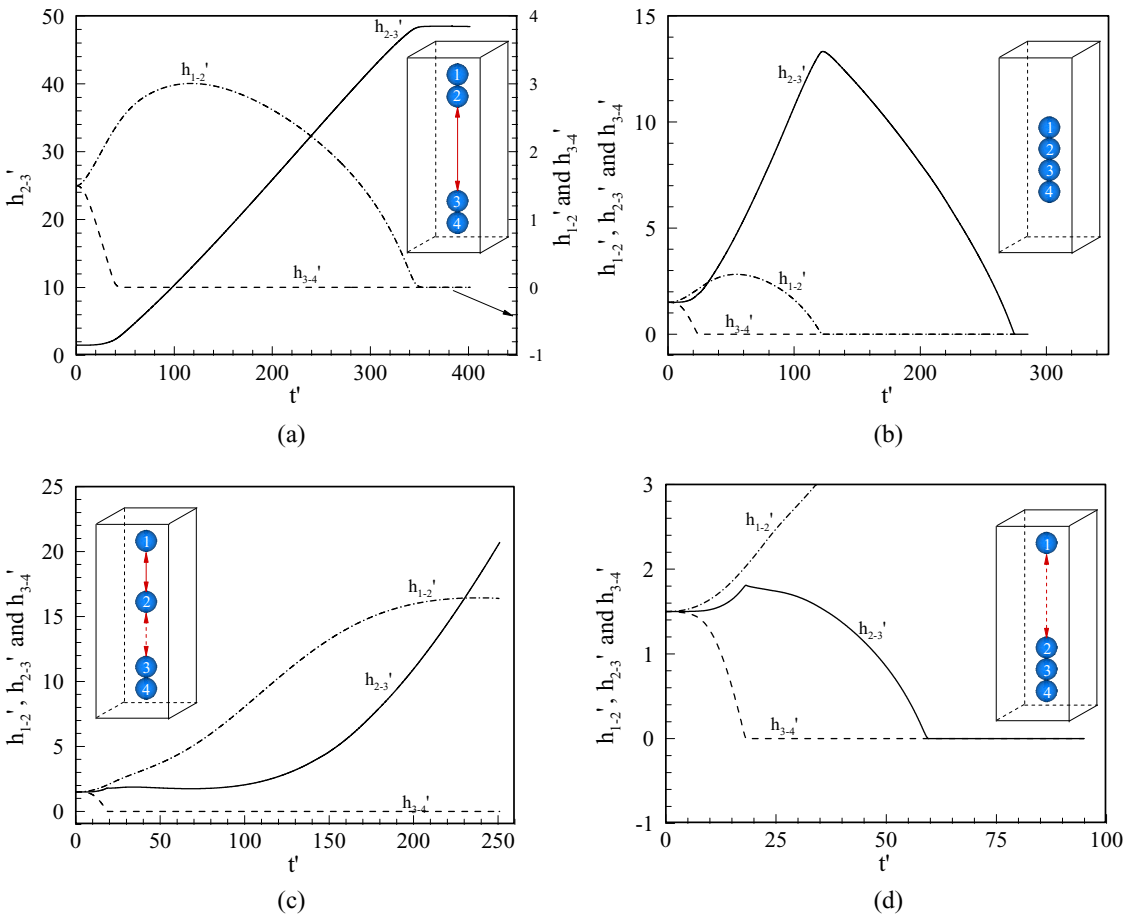

FIG. 8. Time history of normalized separation between neighboring spheres for different grouping behaviors: (a) Re = 14 (GB I), (b) Re = 25 (GB II), (c) Re = 43.5 (GB III), and (d) Re = 50 (GB IV).

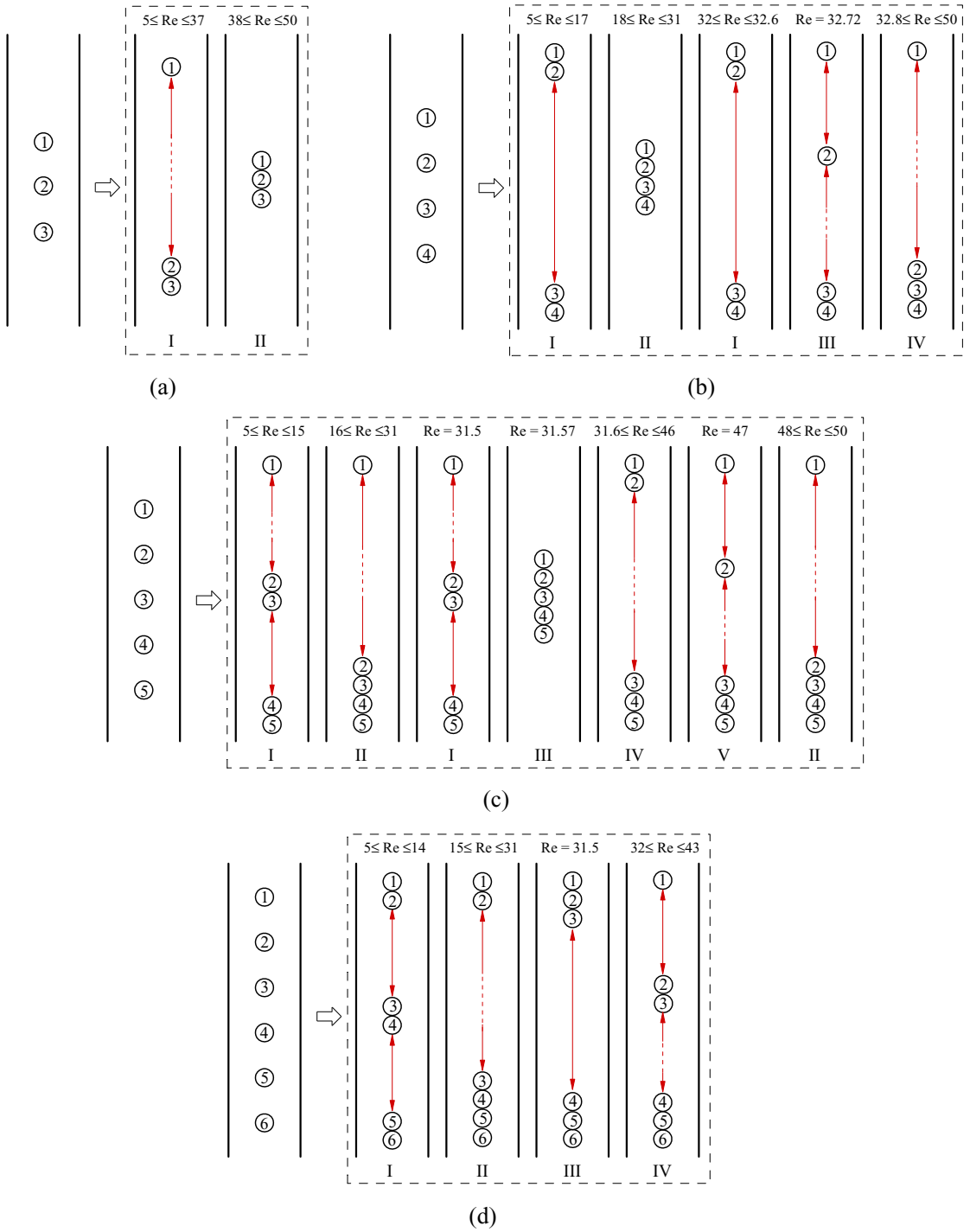

FIG. 9. Summary of grouping behavior as the Reynolds number increases for (a) $n = 3$, (b) $n = 4$, (c) $n = 5$, and (d) $n = 6$. Solid lines with arrows indicate that the distance remains constant, while dashed lines indicate that the distance increases with time.

all the particles are eventually grouped together and settle as a whole unit.

For the case of $n = 6$ shown in Fig. 9(d), four kinds of grouping behavior are observed as the Reynolds number increases. However, we did not observe the grouping of all particles, as can be observed for $n = 3 - 5$. Numerical simulations indicate that this kind of behavior is more likely to happen for large Reynolds numbers or small initial interparticle separations. In view of this we conducted some simulations of the settling of multiple particles at $\mathrm{Re} = 50$ and $h_0' = 0.5$ and show the results in Fig. 10. One can see that the above-mentioned behavior still stands for $n \leqslant 5$. The uppermost particle is always left behind for $n \geqslant 6$. Here it should be mentioned that we present the results of the Reynolds number only up to 43 in Fig. 9(d) because the vertical groups will collapse during settling beyond that, which will be furthered discussed.

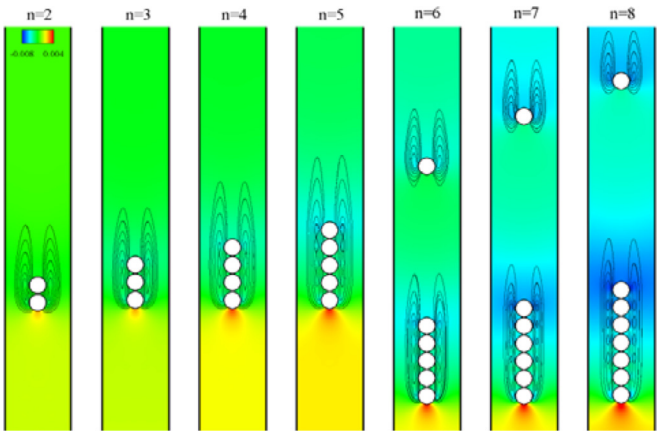

FIG. 10. The grouping behavior for $n = 2-8$ at $\mathrm{Re} = 50$ and $h_0{}' = 0.5$.

Additionally, the grouping behavior is quite similar for all the cases shown in Fig. 9 at low Reynolds numbers. The two lowermost particles always come together first and form a vertical doublet, then the two next particles form another doublet, and so on. Therefore, when n is even we can observe $n/2$ doublets which are kept at finite distances from each other. However, when n is odd, there are $(n-1)/2$ doublets and the uppermost particle is always left behind. To gain deeper insight into this grouping behavior, we also simulated the settling of up to 19 particles, which will be discussed in the next section.

C. The grouping behavior for $n \leqslant 19$ at low Reynolds number

In Fig. 11 we show the instantaneous streamline and pressure distribution of the settling particles for $n = 3-10$ at $\mathrm{Re} = 10$ and $h_0{}' = 1.5$. The computational domain is $4d \times 600d$ for $n > 6$. As mentioned above, the settling behavior is similar for all of these cases. For instance, we can observe three stable doublets for $n = 7$ and four doublets for $n = 9$, as shown in Fig. 11(a). However, when n is even, such as $n = 6$, 8, and 10, it appears in the figure that the two uppermost particles may not contact and form a doublet. To illustrate this, we show the time series of normalized separations between the particles which will contact eventually in Fig. 12. For instance, the case of $n = 6$ shown in Fig. 12(a) confirms that the two lowermost particles (particles 5 and 6) first form a doublet, and then the particles next to the doublet, particles 3 and 4. For the two uppermost particles, particles 1 and 2, one can see that the separation between them increases first and then keeps decreasing slowly. Although Fig. 12 does not show this contact, it presumably takes a long time for $h'_{1\text{-}2}$ to reach zero, which indicates that particles 1 and 2 will contact eventually. The same can be said for the cases of $n = 8$ and $n = 10$.

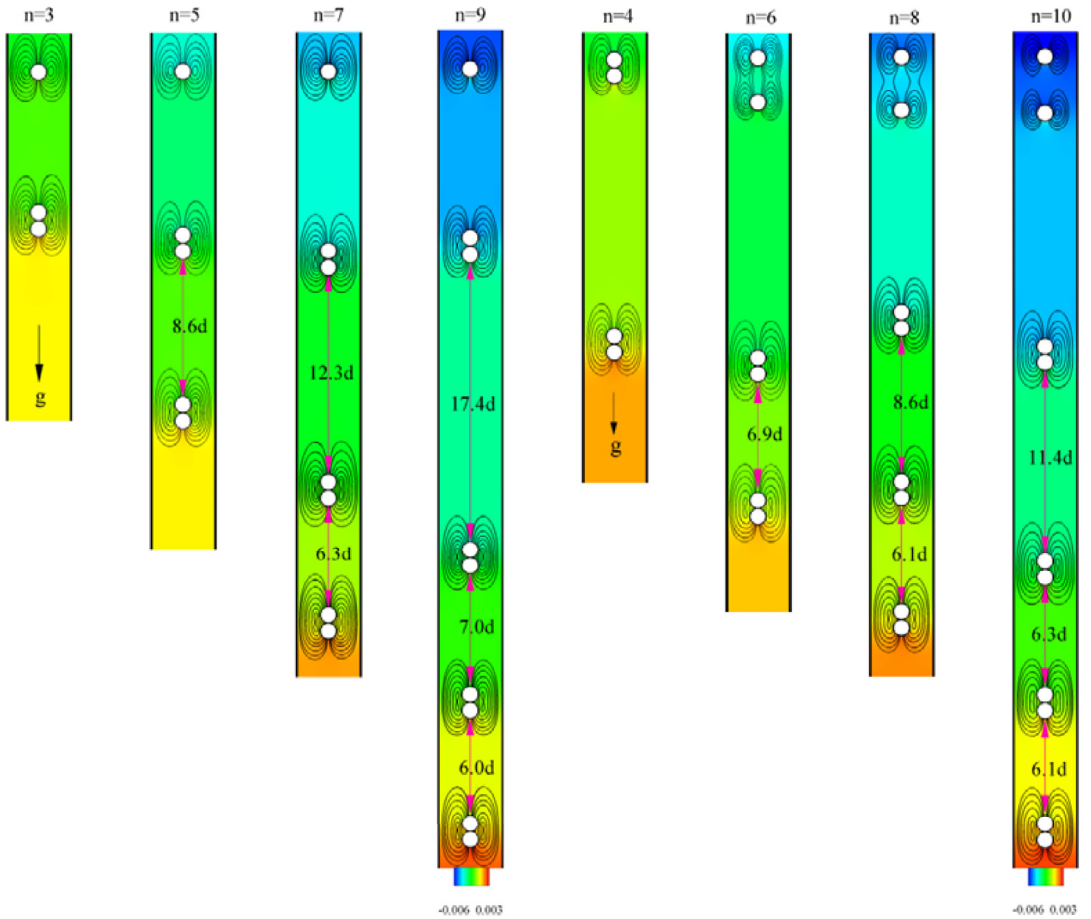

(a) (b)

FIG. 11. The grouping behavior at $\mathrm{Re} = 10$ and $h_0{}' = 1.5$ for (a) $n = 3, 5, 7, 9$ and (b) $n = 4, 6, 8, 10$.

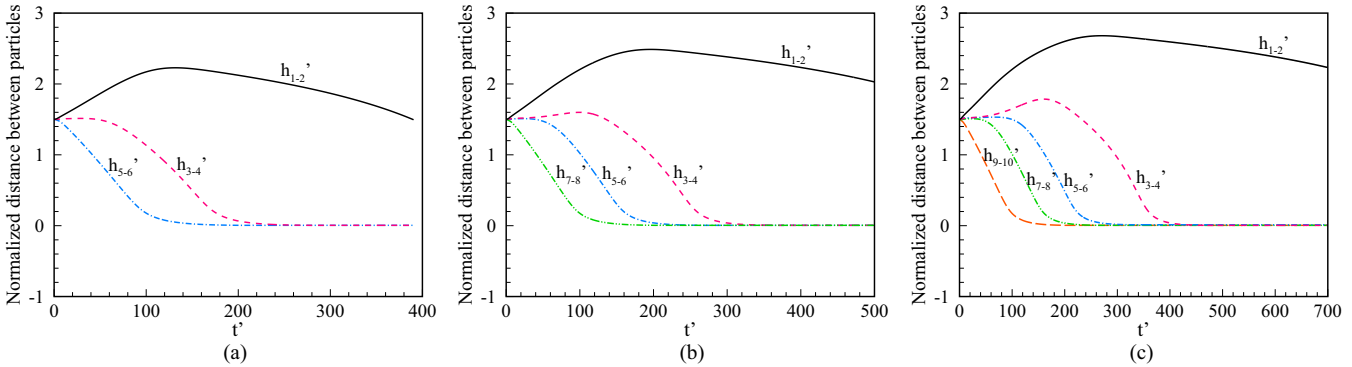

FIG. 12. Time history of normalized separation between particles that form a doublet for (a) $n = 6$, (b) $n = 8$, and (c) $n = 10$.

At steady state, all the doublets settle at the same velocity at low Reynolds numbers, leading to the fact that the distances between doublets remain constant, as shown in Fig. 13. The lower the particle pair is, the less time it takes to form a doublet. This results in a smaller distance between the lower doublets. For instance, $h'_{7\text{-}8}$ is smaller than $h'_{5\text{-}6}$ and $h'_{5\text{-}6}$ is much smaller than $h'_{3\text{-}4}$, as shown in Fig. 13(c).

We show a schematic illustration of the grouping behavior for $n = 5 - 19$ at $\mathrm{Re} = 10$ and $h_0{}' = 1.5$ in Fig. 14. The computational domain is $4d \times 800d$ for $n > 10$. The corresponding results at $\mathrm{Re} = 12$ and $\mathrm{Re} = 13$ for $n = 19$ are also shown. For simplicity, we consider only the case of odd numbers of particles. We observe similar grouping behavior for all cases: the particles form doublets from the bottom upward except for the uppermost particle, which is always left behind. In Fig. 14, we also show the normalized separation between doublets. The separation between the two uppermost doublets is much larger compared with those between others because it takes a very long time for the two uppermost particles to form a doublet, especially when the number of particles is large. We also observe that the separation between doublets decreases from the top to the bottom, which displays a power-law relation, as shown in Fig. 15. This power-law exponent remains constant irrespective of the number of particles when $n \geqslant 13$. It is also interesting that the separation between doublets approaches a constant independent of the number of particles n when $n \geqslant 9$. For instance, the separations are about $6d$ for the lower doublets, as shown in Fig. 14. We believe that this constant depends on the Reynolds number as well as the channel width. For $n = 19$, this separation is $5.6d$ and $5.4d$ for $\mathrm{Re} = 12$ and $\mathrm{Re} = 13$, respectively. The effect of the channel width is not taken into account in this work. However, we still think that the power-law dependence shown in Fig. 15 holds for the finite-width channel. As shown in Fig. 7(b), it is getting hard to observe the grouping behavior GB I when the channel width is increased. The Reynolds number should be very low for large channels. Nevertheless, it is possible that the grouping behavior GB I does not happen at all if the Reynolds number is too low because the particles may settle individually because of negligible inertial effect.

Figure 16 shows the effect of the number of particles on the normalized separation between doublets. We show only the first, second, third, and fourth separations from the top of the settling particles, i.e., $h'_{3\text{-}4}$, $h'_{5\text{-}6}$, $h'_{7\text{-}8}$, and $h'_{9\text{-}10}$.A similar power-law increase is observed for all the results except for $h'_{9\text{-}10}$ as the number of particles increases. We believe that this power-law relation would also be true for the result of $h'_{9\text{-}10}$ if larger n were considered.

As shown in this work, the particles will display certain grouping patterns depending on the Reynolds number and initial conditions if they are coaxially settling in a narrow channel. However, it should be stated here that the grouping patterns will break down eventually after a long enough time (defined as T_c') because of nonlinear inertial effects. The larger the Reynolds number is, and the larger the group is, the sooner the group will collapse. To illustrate this, we show

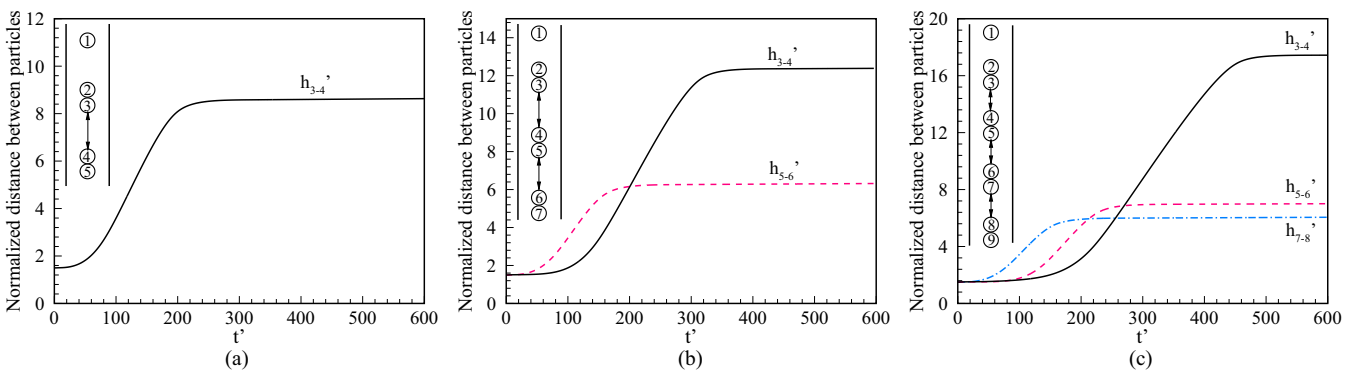

FIG. 13. Time history of normalized separation between the doublets for (a) $n = 5$, (b) $n = 7$, and (c) $n = 9$.

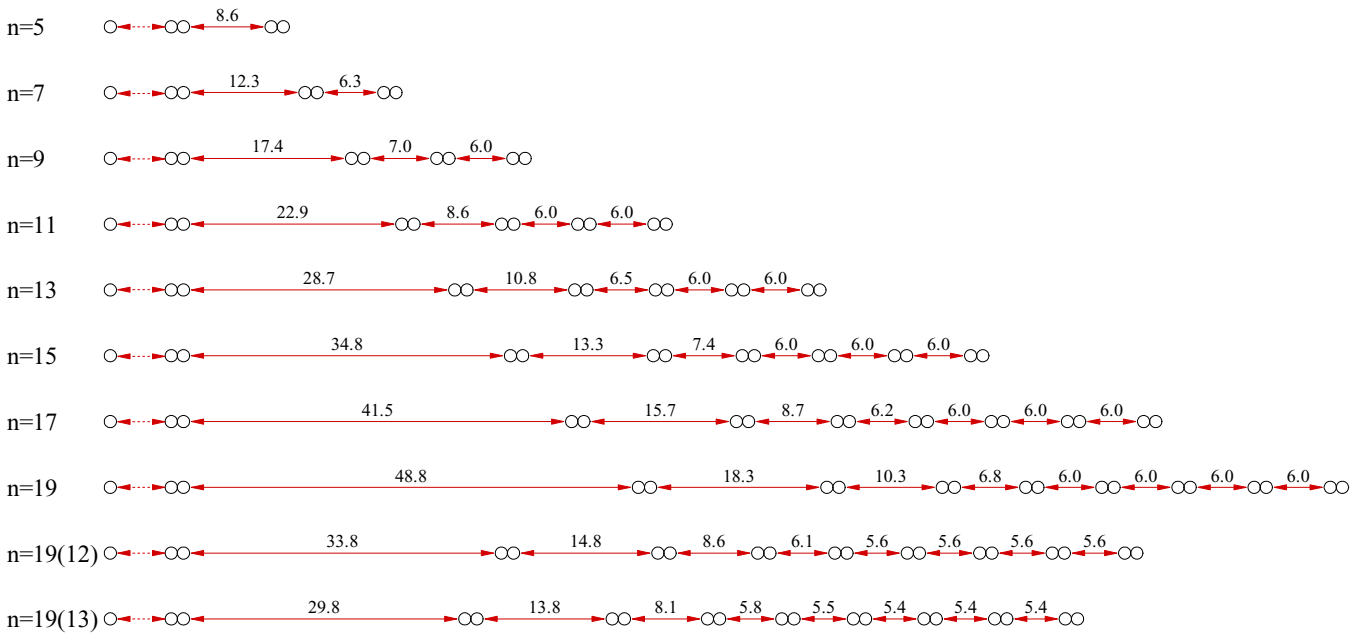

FIG. 14. Schematic illustration of the grouping behavior for $n = 5-19$ at Re $= 10$ and $h_0{}' = 1.5$. In consideration of computational time we consider only the case of odd numbers of particles. The numbers above the red line segments shown in the figure represent the normalized separations between doublets. The results of $n = 19$ at Re $= 12$ and Re $= 13$ are also shown.

the dependence of T_c' on the Reynolds number for $n = 4$ and $h_0' = 0.5$ in Fig. 17, along with the corresponding results of two other computational resolutions: $d = 10$ and $d = 25$. We consider three groups of Reynolds number: Re $= 40, 45$ and 50. Although there is a difference between the values of T_c', the general tendency is similar for all three computational resolutions: the collapse of the particle group takes place earlier for larger Reynolds number. In Fig. 18 we show the streamline and pressure distribution of four particles settling with $h_0' = 0.5$ at Re $= 45$ and Re $= 50$, respectively. In both cases the particles form a four-particle group which settles as a whole for a long time. However, this group begins to collapse at $t' = 184.4$ for Re $= 45$ and at $t' = 166.8$ for Re $= 50$, after which the particles no longer settle as a cohesive group. For the purpose of comparison, we also adopt the lattice Boltzmann method proposed by Lallemand and Luo [30] to deal with the same problem. The results are presented in Fig. 19, which is similar to Fig. 18 in general features. We can observe the same grouping pattern although it takes less time for the group to break down in the simulations. The reason for this is likely due to the fact that these two methods update the distribution functions f_i on the grids close to the particle surfaces differently. However, this is not our concern in the present work.

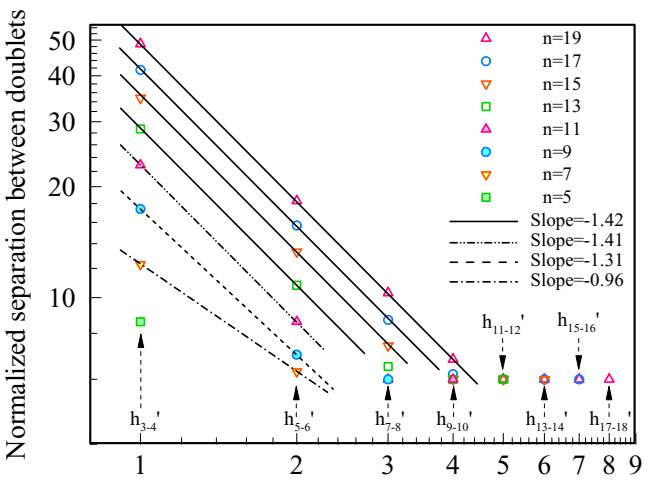

FIG. 15. Power-law decrease of the normalized separation between doublets for Re $= 10$.

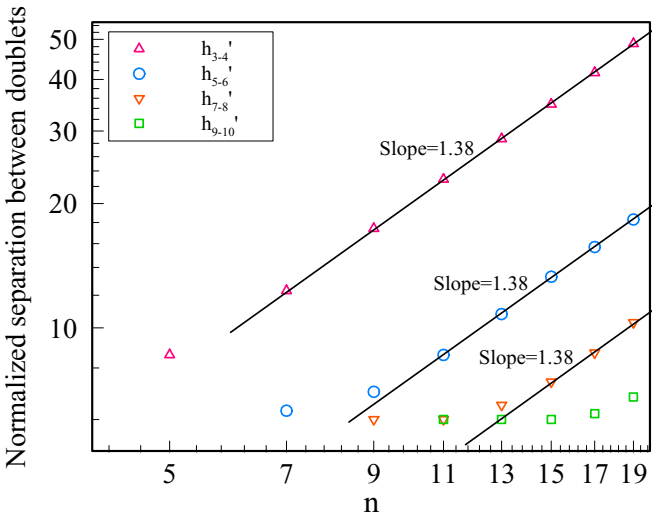

FIG. 16. Normalized separation between doublets as a function of the number of particles for Re $= 10$.

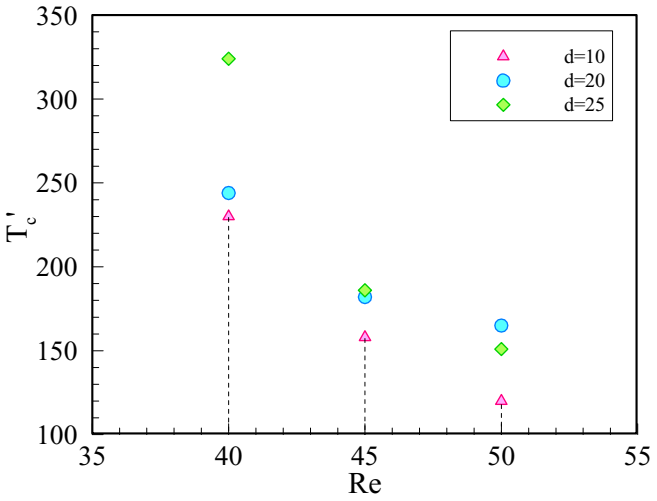

FIG. 17. Dependence of T_c' on the Reynolds number for different computational resolutions at $h_0' = 0.5$. The number of particles is $n = 4$. T_c' is defined as the time it takes for the particle group to collapse.

Finally, we should point out that the choice of collision strategy (the lubrication force [21,29] or the repulsive force [24,31]) may have limited effect on some simulation results such as the final distance between doublets (Fig. 6) or the specific Reynolds number corresponding to GB III behavior (Fig. 7), but it does not alter the essential features of the particles' behavior. This was also demonstrated by our previous work (Nie and Lin [32]).

V. CONCLUSIONS

We have studied, using direct numerical simulation, the grouping behavior of multiple particles settling under the influence of gravity in a narrow channel. The particles are initially coaxially placed with the same interparticle separation. The calculations are based on our LB—DF-FD method. We have focused on the dependence of the particles' behavior on Reynolds number, number of particles, and initial placement. The present method was validated by simulating the sedimentation of two particles in a channel and the resulting DKT motion in two dimensions. We also simulated the sedimentation of a sphere in a square channel for three-dimensional validation.

We presented a detailed study of the grouping behaviors for the case of $n = 4$. It has been shown that four kinds of grouping behavior are observed according to the Reynolds number when the channel width is fixed at $L' = 4$. The particles may settle as one, two, or three groups when Re is varied. In particular, there is a transient behavior (GB III) that rarely occurred and was observed only at a specific Reynolds number, which apparently increased linearly with the initial interparticle separation h_0'. We also examined the wall effects on the settling of particles. There are only two grouping behaviors when the channel width is small, such as $L' < 3.5$. In addition, the GB IV behavior is more likely to take place with larger channel widths, whereas the opposite is true for the GB I behavior.

In addition to $n = 4$ we also studied the grouping behavior for the cases of $n = 3$, 5, and 6 when the channel width is fixed at $L' = 4$. The effect of the number of particles is significant. We can observe only two kinds of behavior for $n = 3$ while five behaviors exist for $n = 5$. It should be mentioned that the vertical array resulting from the particle grouping is more likely to break down when the Reynolds number is larger; therefore, we could not observe the grouping behavior for the case of $n = 6$ when Re > 43.

Finally, we focused on the grouping behavior when the Reynolds number is small. We observed similar behavior irrespective of the number of particles n: the two lowermost particles always come together first and form a vertical doublet, then the two next lowest particles form another doublet, and so on. Eventually, we observed $n/2$ doublets when n is even, and $(n-1)/2$ doublets when n is odd. The separations between these doublets remain constant, and show a power-law increase from the top to the bottom.

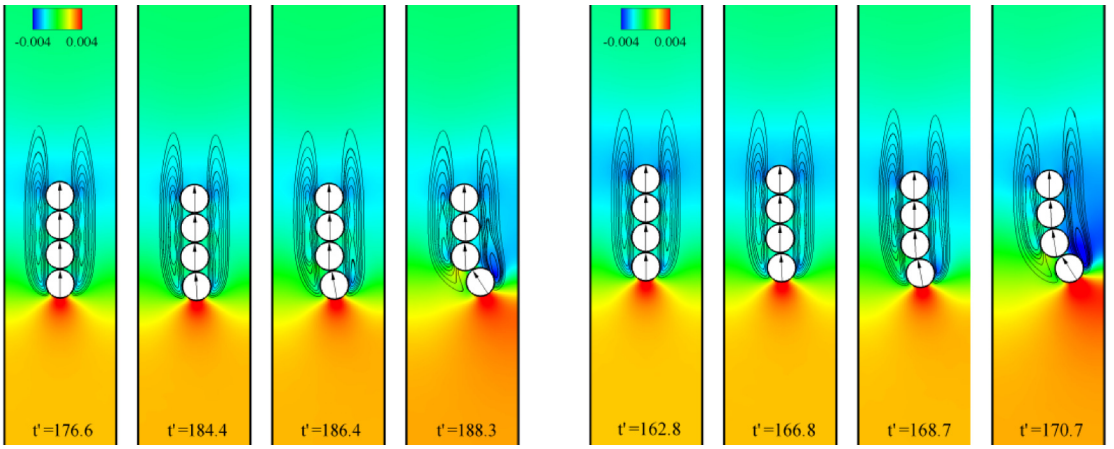

(a) (b)

FIG. 18. Streamline and pressure distribution for particles settling with $h_0' = 0.5$ at (a) Re = 45 and (b) Re = 50. The black arrow on each particle indicates its rotation, with a vertical orientation at the outset.

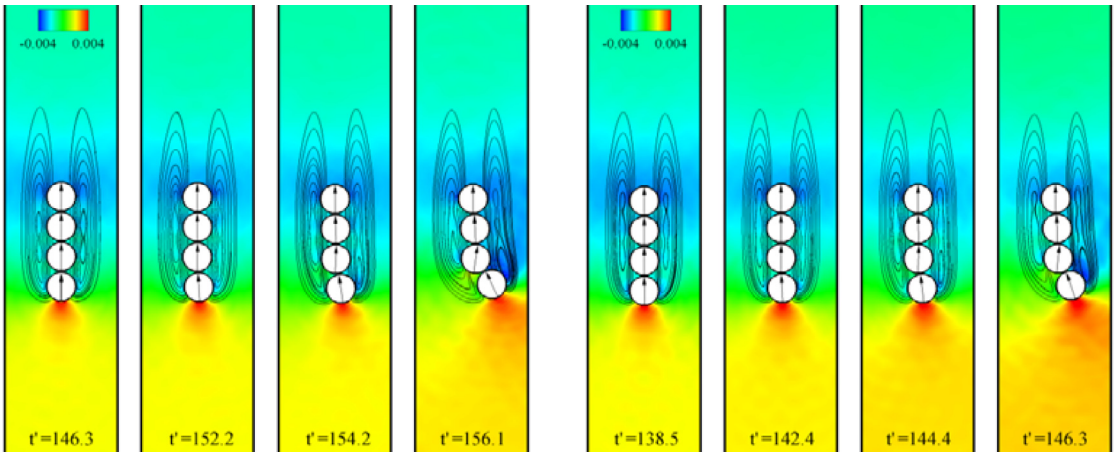

(a) (b)

FIG. 19. Similar results to those in Fig. 18 obtained through the lattice Boltzmann method by Lallemand and Luo [30]: (a) Re = 45 and (b) Re = 50. The parameters are identical to those of Fig. 18.

ACKNOWLEDGMENTS

This work was supported by the National Natural Science Foundation of China (Grant No. 11272302) and its Major Program (Grant No. 11132008). This work was also supported by the Zhejiang Provincial Natural Science Foundation of China (Grant No. LY15A020004).

[1] T.-W. Pan, D. D. Joseph, R. Bai, R. Glowinski, and V. Sarin, Fluidization of 1204 spheres: simulation and experiment, J. Fluid Mech. **451**, 169 (2002).

[2] M. Jenny, J. Dušek, and G. Bouchet, Instabilities and transition of a sphere falling or ascending freely in a Newtonian fluid, J. Fluid Mech. **508**, 201 (2004).

[3] W. B. Daniel, R. E. Ecke, G. Subramanian, and D. Koch, Clusters of sedimenting high-Reynolds-number particles, J. Fluid Mech. **625**, 371 (2009).

[4] Z. H. Xia, K. W. Connington, S. Rapaka, P. T. Yue, J. J. Feng, and S. Y. Chen, Flow patterns in the sedimentation of an elliptical particle, J. Fluid Mech. **625**, 249 (2009).

[5] A. E. Yacoubi, S. Xu, and Z. J. Wang, Computational study of the interaction of freely moving particles at intermediate Reynolds numbers, J. Fluid Mech. **705**, 134 (2012).

[6] H. B. Huang, X. Yang, and X.-Y. Lu, Sedimentation of an ellipsoidal particle in narrow tubes, Phys. Fluids **26**, 053302 (2014).

[7] D. M. Nie, J. Z. Lin, and M. J. Zheng, Direct numerical simulation of multiple particles sedimentation at an intermediate Reynolds number, Commun. Comput. Phys. **16**, 675 (2014).

[8] M. J. Riddle, C. Narvaez, and R. B. Bird, Interactions between two spheres falling along their line of centers in a viscoelastic fluid, J. Non-Newtonian Fluid Mech. **2**, 23 (1977).

[9] J. Feng, P. Y. Huang, and D. D. Joseph, Dynamic simulation of sedimentation of solid particles in an Oldroyd-B fluid, J. Non-Newtonian Fluid Mech., **63**, 63 (1996).

[10] S. Daugan, L. Talini, B. Herzhaft, and C. Allain, Aggregation of particles settling in shear-thinning fluids. Part 1. Two-particle aggregation, Eur. Phys. J. E **7**, 73 (2002).

[11] S. Daugan, L. Talini, B. Herzhaft, and C. Allain, Aggregation of particles settling in shear-thinning fluids. Part 2. Three-particle aggregation, Eur. Phys. J. E **9**, 55 (2002).

[12] J. Hao, T.-W. Pan, R. Glowinski, and D. D. Joseph, A fictitious domain distributed Lagrange multiplier method for the particulate flow of Oldroyd-B fluids, J. Non-Newtonian Fluid Mech. **156**, 95 (2009).

[13] J. Michele, R. Pätzold, and R. Donis, Alignment and aggregation effects in suspensions of spheres in non-Newtonian media, Rheol. Acta **16**, 317 (1977).

[14] D. Won and C. Kim, Alignment and aggregation of spherical particles in viscoelastic fluid under shear flow, J. Non-Newtonian Fluid Mech. **117**, 141 (2004).

[15] A. Mirsepassi, B. Rajaram, A. Mohraz, and D. Dunn-Rankin, Particle chaining and chain dynamics in viscoelastic liquids, J. Non-Newtonian Fluid Mech. **179–180**, 1 (2012).

[16] R. Pasquino, G. D'Avino, P. L. Maffettone, F. Greco, and N. Grizzuti, Migration and chaining of noncolloidal spheres suspended in a sheared viscoelastic medium. Experiments and numerical simulations, J. Non-Newtonian Fluid Mech. **203**, 1 (2014).

[17] J. Happel and H. Brenner, *Low Reynolds Number Hydrodynamics* (Mantinus Nijhoff, Dordrecht, 1973).

[18] D. M. Nie and J. Z. Lin, A LB-DF/FD method for particle suspensions, Commun. Comput. Phys. **7**, 544 (2010).

[19] Y. H. Qian, Lattice BGK models for Navier-Stokes equation, Europhys. Lett. **17**, 479 (1992).

[20] Z. S. Yu and X. M. Shao, A direct-forcing fictitious domain method for particulate flows, J. Comput. Phys. **227**, 292 (2007).

[21] J. Kromkamp, D. van den Ende, D. Kandhai, R. van der Sman, and R. Boom, Lattice Boltzmann simulation of 2D and 3D

non-Brownian suspensions in Couette flow, Chem. Eng. Sci. **61**, 858 (2006).

[22] N.-Q. Nguyen and A. J. C. Ladd, Lubrication corrections for lattice-Boltzmann simulations of particle suspensions, Phys. Rev. E **66**, 046708 (2002).

[23] Z. G. Feng and E. E. Michaelides, The immersed boundary-lattice Boltzmann method for solving fluid-particles interaction problems, J. Comput. Phys. **195**, 602 (2004).

[24] R. Glowinski, T.-W. Pan, T. I. Hesla, D. D. Joseph, and J. Periaux, A fictitious domain approach to the direct numerical simulation of incompressible viscous flow past moving rigid bodies: Application to particulate flow, J. Comput. Phys. **169**, 363 (2001).

[25] A. Miyamura, S. Iwasaki, and T. Ishii, Experiment wall correction factors of single solid spheres in triangular and square cylinders, and parallel plates, Int. J. Multi-phase Flow **7**, 41 (1981).

[26] C. K. Aidun, Y. Lu, and E. Ding, Direct analysis of particulate suspensions with inertia using the discrete Boltzmann equation, J. Fluid Mech. **373**, 287 (1998).

[27] R. Clift, J. R Grace, and M. E. Weber, *Bubbles, Drops, and Particles* (Academic Press, New York, 1978).

[28] Z. Yu, N. Phan-Thien, and R. I. Tanner, Dynamical simulation of sphere motion in a vertical tube, J. Fluid Mech. **518**, 61 (2004).

[29] X. Yuan and R. Ball, Rheology of hydrodynamically interacting concentrated hard disks, J. Chem. Phys. **101**, 9016 (1994).

[30] P. Lallemand and L.-S. Luo, Lattice Boltzmann method for moving boundaries, J. Comput. Phys. **184**, 406 (2003).

[31] D. Wan and S. Turek, An efficient multigrid-FEM method for the simulation of solid–liquid two phase flows, J. Comput. Appl. Math. **203**, 561 (2007).

[32] D. M. Nie and J. Z. Lin, Behavior of three circular particles in a confined power-law fluid under shear, J. Non-Newtonian Fluid Mech. **221**, 76 (2015).